ESC European Society of Cardiology

European Heart Journal (2019) **00**, 1–10
doi:10.1093/eurheartj/ehz467

ESC GUIDELINES

2019 ESC Guidelines for the management of patients with supraventricular tachycardia: supplementary data

The Task Force for the 2019 European Society of Cardiology (ESC) Guidelines for the management of patients with supraventricular tachycardia

Developed in collaboration with the Association for European Paediatric and Congenital Cardiology (AEPC)

Authors/Task Force Members: Josep Brugada* (Chairperson) (Spain), Demosthenes G. Katritsis* (Chairperson) (Greece), Elena Arbelo (Spain), Fernando Arribas (Spain), Jeroen J. Bax (Netherlands), Carina Blomström-Lundqvist (Sweden), Hugh Calkins (United States of America), Andrew Coats (United Kingdom), Domenico Corrado (Italy), Spyridon G. Deftereos (Greece), Gerhard-Paul Diller (Germany), Juan J. Gomez-Doblas (Spain), Bulent Gorenek (Turkey), Andrew Grace (United Kingdom), Siew Yen Ho (United Kingdom), Juan-Carlos Kaski (United Kingdom),

*Corresponding authors: Josep Brugada, Cardiology Department, Hospital Clinic, and Pediatric Arrhythmia Unit, Hospital Sant Joan de Déu, University of Barcelona, Spain. Tel: +34 3460 902 2351, Fax: +34 3493 227 1777, Email: jbrugada@clinic.cat.

Demosthenes G. Katritsis, Deaprtment of Cardiology, Hygeia Hospital, E. Stavrou 4, 15123 Athens, Greece, Tel: +30 6944 845 505, Fax: +30 210 6722535, Email: dkatrits@dgkatritsis.gr.

[1]**Representing the AEPC.**

ESC entities having participated in the development of this document:

Associations: Acute Cardiovascular Care Association (ACCA), European Association of Cardiovascular Imaging (EACVI), European Association of Preventive Cardiology (EAPC), European Heart Rhythm Association (EHRA), Heart Failure Association (HFA).

Councils: Council for Cardiology Practice.

Working Groups: Cardiac Cellular Electrophysiology, Cardiovascular Pharmacotherapy, Cardiovascular Surgery, Development Anatomy and Pathology, Grown-up Congenital Heart Disease.

Karl-Heinz Kuck (Germany), Pier David Lambiase (United Kingdom), Frédéric Sacher (France), Georgia Sarquella-Brugada[1] (Spain), Piotr Suwalski (Poland), Antonio Zaza (Italy)

Document Reviewers: Tom De Potter [Committee for Practice Guidelines (CPG) Review Co-ordinator] (Belgium), Christian Sticherling (CPG Review Co-ordinator) (Switzerland), Victor Aboyans (France), Cristina Basso (Italy), Mario Bocchiardo (Italy), Werner Budts (Belgium), Victoria Delgado (Netherlands), Dobromir Dobrev (Germany), Donna Fitzsimons (United Kingdom), Sofie Gevaert (Belgium), Hein Heidbuchel (Belgium), Gerhard Hindricks (Germany), Peter Hlivak (Slovakia), Prapa Kanagaratnam (United Kingdom), Hugo Katus (Germany), Josef Kautzner (Czech Republic), Thomas Kriebel[1] (Germany), Patrizio Lancellotti (Belgium), Ulf Landmesser (Germany), Christophe Leclercq (France), Basil Lewis (Israel), Yuri Lopatin (Russian Federation), Béla Merkely (Hungary), Thomas Paul (Germany), Nikola Pavlovic (Croatia), Steffen Petersen (United Kingdom), Anna Sonia Petronio (Italy), Tatjana Potpara (Serbia), Marco Roffi (Switzerland), Daniel Scherr (Austria), Evgeny Shlyakhto (Russian Federation), Iain A. Simpson (United Kingdom), Katja Zeppenfeld (Netherlands)

The disclosure forms of all experts involved in the development of these Guidelines are available on the ESC website www.escardio.org/guidelines

Keywords Guidelines • arrhythmia • tachycardia • supraventricular • flutter • atrioventricular • re-entrant • focal • macro–re-entrant • junctional • nodal • pre-excitation • ablation

Table of contents

List of figures

1 Electrophysiological mechanisms of supraventricular tachycardia

1.1 Mechanisms of non-re-entrant arrhythmias

Automaticity is normally suppressed in non-pacemaking myocytes by hyperpolarizing membrane currents (I_{K1} or I_{KACh}) that keep diastolic potential constant. In addition, non-pacemaking myocytes scantily express a diastolic depolarizing current (I_f), a significant contributor—along with I_{CaL} (L-type Ca^{2+} current)—to the physiological automaticity of the sinoatrial (SAN) and atrioventricular (AVN) nodes. In non-pacemaking myocytes, an imbalance between hyperpolarizing and depolarizing diastolic currents can occur under pathological conditions, and lead to enhanced automaticity (EA).[1] In this case, the abnormality is intrinsic to the cell membrane, i.e. it resides in (primary or secondary) dysfunction of sarcolemmal ion channels. Albeit potentially modulated by excitation of surrounding tissue, firing of automatic myocytes is independent and, therefore, automatic rhythms are typically dissociated from the basic one and are characterized by variable coupling intervals. EA is facilitated by partial

membrane depolarization (e.g. by ischaemia), hypokalaemia, and sympathetic activation, which disrupt the balance between hyperpolarizing and depolarizing diastolic currents.

After-depolarizations may occur during the action potential [early after-depolarizations (EADs)], or during diastole [delayed after-depolarizations (DADs)] (*Supplementary Figure 1*). Arrhythmias caused by after-depolarizations are named 'triggered activity' (TA) because, unlike abnormal automaticity, they are often related to a previous excitation that sets the conditions for their occurrence. EADs are classically due to partial I_{CaL} recovery and reactivation during the action potential.[1] This is facilitated by repolarization slowing (long QT), but also by a loss of a proper plateau phase (action potential 'triangulation'), thus explaining why EADs may also occur in atria.[2] I_{CaL} reactivation causes a membrane potential oscillation, which, if arising at a sufficiently negative membrane potential (phase 3 EADs), may activate surrounding myocytes or, in the case of phase 2 EADs, further delay repolarization. Although promoted by bradycardia, EADs are also enhanced by adrenergic stimulation. DADs are generated by diastolic Ca^{2+} release from the sarcoplasmic reticulum (SR), its intracellular store, to form intracellular 'Ca^{2+} waves'.[1,3] A rise in cytosolic Ca^{2+} activates Ca^{2+}-sensitive membrane currents (mainly I_{NCX}) resulting in membrane potential (*Supplementary Figure 1*). Ca^{2+} waves occur when SR stability is compromised by excessive Ca^{2+} loading, or when opening of SR Ca^{2+} channels (RyRs) is enhanced.[3] Thus, DADs are facilitated by tachycardia and adrenergic stimulation. Under specific conditions, Ca^{2+} waves may occur during the action potential, thus inducing EADs instead.[3] If large enough, phase 3 EADs and DADs can directly excite the myocardium (TA). Even if they fail do so, EADs result in strong repolarization heterogeneity, thus promoting 're-entry'.[2]

A further factor in the genesis of non-re-entrant arrhythmias is electrical coupling between the focus of origin and the surrounding tissue. Electrical coupling through 'gap junctions' guarantees silencing of unstable tissue by the surrounding stable one; therefore, partial uncoupling (e.g. by fibrosis) may unveil membrane potential instability. On the other hand, propagation of automatic/TA requires the excitation of the adjacent tissue, which implies some degree of electrical coupling and I_{Na} availability.

Some system components are implicated in both EA and TA, thus making the two mechanisms similarly responsive to some

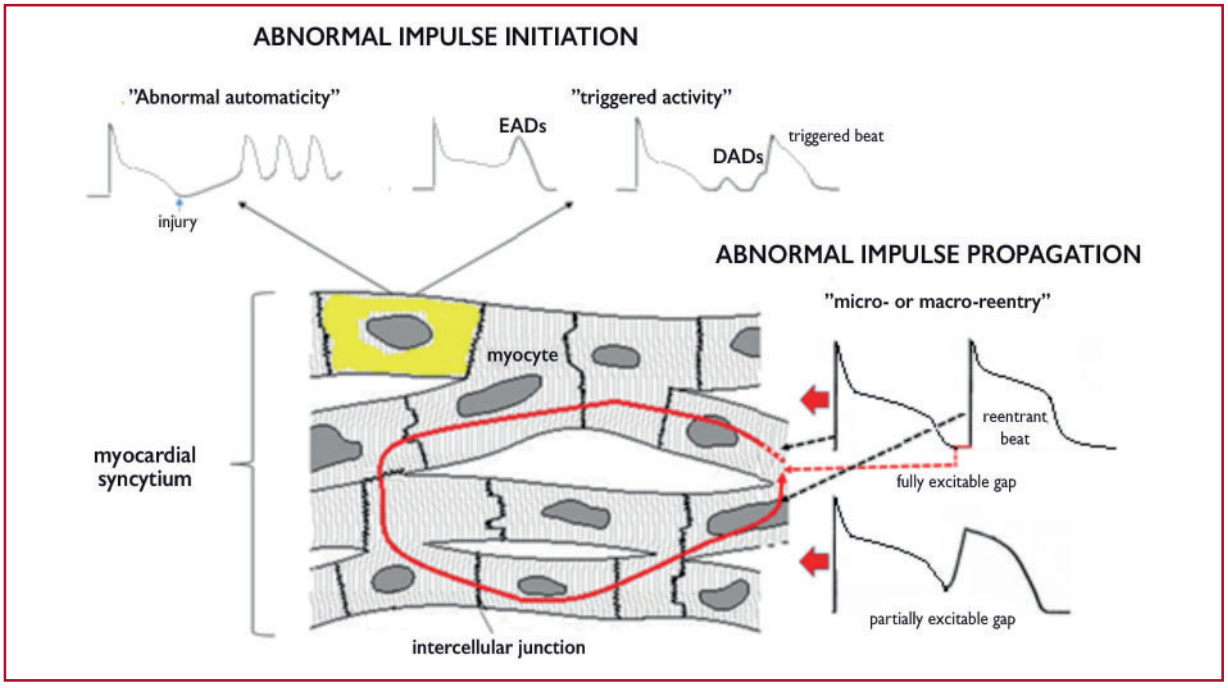

Supplementary Figure 1 Mechanisms of arrhythmogenesis. Abnormal impulse initiation: the cardiac impulse may be theoretically initiated by a single myocyte (in yellow); this is the case for abnormal (enhanced) automaticity *and triggered activity*. Whereas abnormal automaticity involves progressive membrane depolarization during the diastole, triggered activity is generated by membrane potential oscillations occurring during the action potential (early after-depolarizations) or the diastolic interval (delayed after-depolarizations) (see text). Abnormal impulse propagation: ectopic self-activation of the heart is caused by circulation of the impulse along a circuit (red line), formed by multiple connected myocytes under specific conditions (see text). The circuit head and tail may be separated by a fully excitable gap if the propagation time is adequate for full recovery of excitability; when the circuit head impinges on partially refractory tissue (a partially excitable gap), further propagation may be slowed, thus allowing circuit perpetuation. Because of conduction anisotropy, fully and partially excitable gaps may coexist within a circuit.
DADs = delayed after-depolarizations; EADs = early after-depolarizations.

interventions. A good example is I_{CaL}, which directly contributes to automaticity, EADs, and SR loading; accordingly, both EA and TA are enhanced by adrenergic activation and suppressed by I_{CaL} blockade. Thus, in terms of response to drugs, EA and TA may not be sharply discriminated; nonetheless, it would be useful to recognize the contribution of SR instability to arrhythmogenesis because it might assist in optimizing drug therapy. For instance, while beta-blockade may be indicated in both EA- and EAD-based TA, carvedilol is the only beta-blocker that seems to stabilize the SR (by inhibiting RyR channels).[3]

1.2 Re-entry

Propagation in the myocardium can occur, albeit with different velocities (anisotropy), in all directions. Thus, given appropriate conditions, regions activated later in propagation may re-excite regions that have already recovered excitability. This phenomenon requires several conditions to be present:[1]

(1) ***An area of unexcitable tissue (obstacle) that splits propagation into two fronts***. The obstacle can be an 'anatomical' structure [valve orifices, dual AVN or accessory pathways (APs), scar tissue, etc.] or even 'functional' (e.g. collision of centripetal fronts emanating from the circuit).

(2) ***Conditions preventing mutual extinction of the two fronts by head-to-head or head-to-tail collision***. 'Unidirectional' conduction, in at least part of the circuit, prevents head-to-head collision. Head-to-tail collision is prevented by a refractory period shorter than the time required by the front to circumnavigate the obstacle (*Supplementary Figure 2*). Accordingly, the minimum circuit length theoretically achievable [commonly named wavelength (WL)] depends on myocardial properties as follows, where CV is conduction velocity:

$$WL = CV \times RP$$

The smaller the WL, the more likely re-entry is to occur; accordingly, either conduction slowing or decreased refractoriness facilitate re-entry. Albeit reality may be more complex, this simple concept is pivotal in understanding antiarrhythmic therapy.

The WL concept is based on the mode of re-entry first described and named 'leading circle' (*Supplementary Figure 2*);[1] nonetheless, functional re-entry may also take the form of 'spiral wave'.[4] While too complex to be described here, spiral waves have been implicated in atrial fibrillation (AF), and their properties are best suited to explain the high arrhythmia rate and the antiarrhythmic efficacy of Na^+ channel blockers.

1.3 Distinguishing re-entrant from non-re-entrant arrhythmias

Supraventricular rhythms with specific electrocardiographic (ECG) patterns [e.g. atrial flutter, atrioventricular nodal re-entrant tachycardia (AVNRT), and atrioventricular re-entrant tachycardia (AVRT)] are caused by re-entry over well-defined anatomical structures; therefore, once the rhythm diagnosis is made, re-entry can be safely assumed as the mechanism. However, this is not the case for focal atrial tachycardias (ATs), in which both re-entry and EA/TA may be involved.[5] Because re-entrant circuits may be microscopic or simulate foci by surface

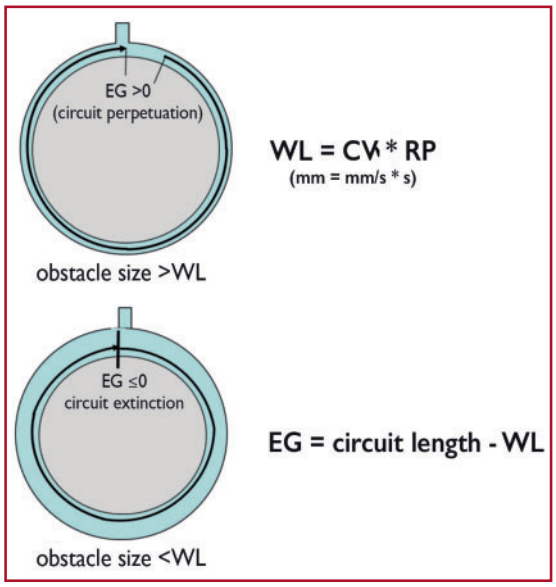

Supplementary Figure 2 Re-entry 'wavelength'. The activation front travels around the obstacle (anatomical or functional). For re-entry to continue, the circuit length (set by anatomical obstacle size or tissue functional properties) must be larger than the wavelength. In this case, an excitable gap separates the circuit head from its tail. If the circuit length is smaller than the wavelength, the circuit head collides with the tail (no excitable gap) and propagation is extinguished. CV = conduction velocity; EG = excitable gap; RP = absolute refractory period; WL = wavelength.

'breakthrough' of transmural propagation, even high-resolution mapping may be inadequate to distinguish them from non-re-entrant activity. However, an educated guess can be made from the response to vagal manoeuvres, adenosine, adrenergic agonist/antagonists, and pacing protocols.[1,5]

1.4 Specificities in anatomy and function of supraventricular structures

Structural specificities may contribute to atrial arrhythmogenesis.[6] For instance, automatic/TA in venous sleeves is facilitated by very thin and poorly coupled myocardium, dual AVN anatomy is pivotal in the genesis of AVNRT, and strong anisotropy supports preferential propagation pathways in atrial flutter. The action potential of atrial 'working' myocytes has a prominent phase 1 repolarization, which makes it more 'triangular' than the ventricular potential. Impulse propagation is supported by I_{Na} in atrial 'working' myocytes, and by I_{CaL} in SAN and AVN myocytes. Accordingly, a sharp response of propagation to I_{CaL} inhibition (via I_{CaL} blockade, beta-blockade, or adenosine) is peculiar to nodal tissue, whereas effective interruption of a primarily nodal arrhythmia by I_{Na} blockade may suggest involvement of atrial tissue in the circuit. Several ionic currents are selectively (or predominantly) expressed in supraventricular myocytes.[6] I_{to} and I_{Kur}, depolarization-activated K^+ currents, account for the triangular shape of the atrial action potential, and voltage-independent SK (Ca^{2+}-activated) and TASK (two-pore) K^+ channels also contribute to speed atrial repolarization.[7,8] I_{KACh}, the atrially located

analogue of the ventricular diastolic current I_{K1}, is activated by acetylcholine or adenosine; it accounts for the suppression of automaticity and repolarization shortening by vagal activation. Notably, the pacemaker current I_f, typical of the SAN, is also weakly expressed in working atrial myocytes and may support EA when enhanced by sympathetic activation. Furthermore, features of atrial I_{Na} make it exquisitely sensitive to some blockers (e.g. ranolazine).[9] These differences underpin the atrial selectivity of some drug effects.

1.5 Arrhythmia mechanism and response to therapy

Each arrhythmia type can be terminated by multiple mechanisms; hence, there is no strict relationship between arrhythmia type and response to interventions. Furthermore, each drug has multiple relevant actions. Thus, putatively effective 'actions', but not 'drugs', should be associated with each arrhythmia mechanism.

Automatic/triggered arrhythmias are logically suppressed by inhibiting their initiation (I_{CaL} blockade, beta-blockade, drug actions stabilizing the SR,[3] or focus ablation), but their propagation may also be prevented (I_{Na} blockade or focus encircling). Re-entrant arrhythmias are suppressed by discontinuing the circuit. This is achieved physically by ablation or pharmacologically with drugs that prolong refractoriness (*Supplementary Figure 2*). To this end, it should be stressed that refractoriness may be prolonged beyond repolarization by Na^+ channel blockers characterized by slow 'off kinetics' (class Ic action, e.g. flecainide).[10] Disease-related membrane depolarization may slow down the 'off kinetics' of intrinsically 'faster' drugs (e.g. lidocaine in ischaemia).[11] Therefore, refractoriness prolongation does not require prolonged repolarization, i.e. it is not an exclusive response to K^+ channel blockade (class III action). If nodal structures are involved, re-entry can be prevented by interventions inhibiting I_{CaL} (I_{CaL} blockade, beta-blockade, and adenosine).

Haemodynamically well-tolerated, myocardial activation at inappropriately high rates maintained over long periods may lead to changes in myocyte function and tissue structure, collectively named 'remodelling'. Once remodelling has occurred, it may facilitate arrhythmias and impair contractile function (tachycardiomyopathy).

2 Tachycardia circuits

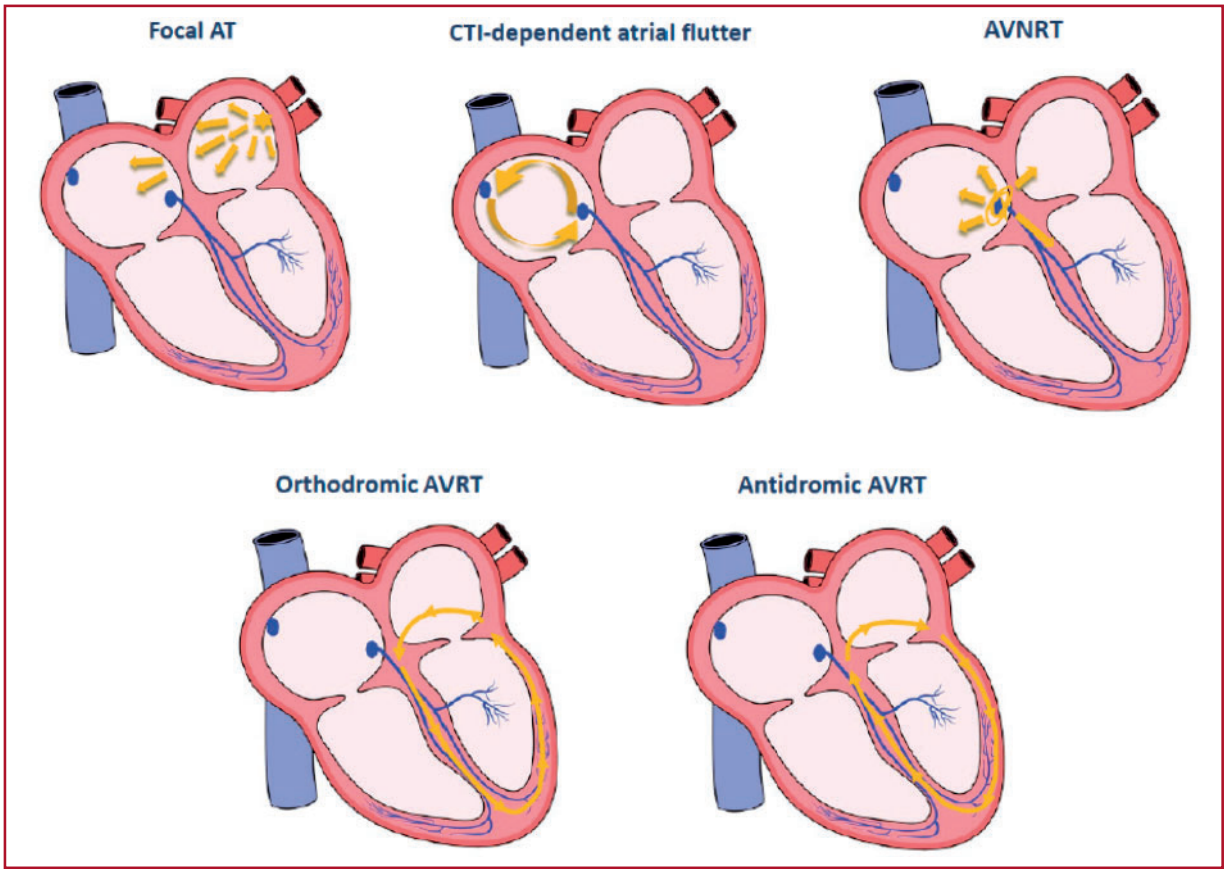

Supplementary Figure 3 Tachycardia circuit in different types of narrow QRS tachycardia. The sinus node, atrioventricular node, and right and left bundle branches are depicted. Internodal tracts have not been anatomically demonstrated. The activation from the sinus node spreads through the atrial myocardium to the atrioventricular node. AT = atrial tachycardia; AVNRT = atrioventricular nodal re-entrant tachycardia; AVRT = atrioventricular re-entrant tachycardia; CTI = cavotricuspid isthmus.

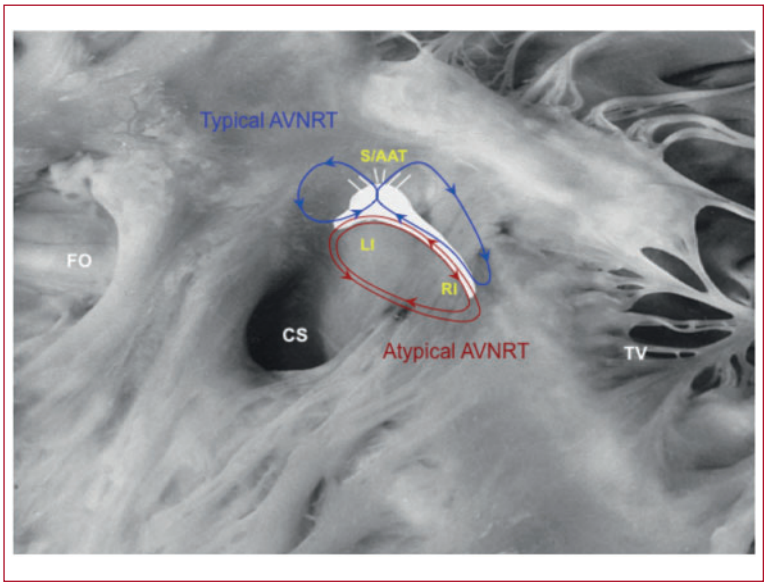

Supplementary Figure 4 Proposed circuit of atrioventricular nodal re-entrant tachycardia. During typical atrioventricular nodal re-entrant tachycardia (slow–fast), right- or left-sided circuits may occur with antegrade conduction through the inferior inputs, and retrograde conduction through the superior inputs or the anisotropic atrionodal transitional area. In atypical atrioventricular nodal re-entrant tachycardia, conduction occurs antegradely through one of the inferior inputs, left or right, and retrogradely through the other one. Depending on the orientation of the circuit, one may record the so-called fast-slow, slow-slow, or indeterminate types. Reproduced with permission from Katritsis DG *et al.*[12] AAT = anisotropic atrionodal transitional area; AVNRT = atrioventricular nodal re-entrant tachycardia; CS = coronary sinus; FO = foramen ovale; LI = left input; RI = right input; S = superior input; TV = tricuspid valve.

3 Cardiac anatomy for the electrophysiologist

3.1 Right atrium

A large triangular-shaped appendage dominates this chamber, occupying its anterior and lateral parts. Internally, the appendage wall is lined by pectinate muscles that extend from the terminal crest to reach the smooth vestibule surrounding the tricuspid valve orifice (*Supplementary Figure 6*).[14]

In the anterior wall, the larger pectinate muscles are arranged nearly in parallel fashion, with thinner branches in between, leaving areas of very thin atrial wall.[15] The terminal crest sweeps like a twisted C-shape, originating from the septal wall, marking the anterior border of the superior caval vein entrance before descending posteriorly and laterally, and then turning anteriorly to skirt to the right side of the Eustachian valve that guards the entrance of the inferior caval vein. Its distal ramifications join with the vestibule toward the orifice of the coronary sinus to form the cavotricuspid (flutter) isthmus, lies between the entrance of the inferior caval vein and the tricuspid annulus (*Supplementary Figure 6*).

The posterior portion of the isthmus is pouch-like in ~10% of patients.[16] The terminal crest marks the border between the smooth intercaval posterior wall of the right atrium (RA) and the appendage.

3.1.1 Non-invasive imaging of the right atrium

In patients with supraventricular tachycardia, non-invasive imaging can provide useful information when structural (anatomical) and/or functional abnormalities are present in the atria, with more experience available for the left atrium (LA) than the RA.[17]

3.1.1.1 Anatomical parameters

RA size, area, and volume are routinely assessed from standard two-dimensional (2D) echocardiography at the end of left ventricular (LV) systole, just before tricuspid valve opening, providing the maximum size/volume. RA size is derived from the apical four-chamber view.[18] The major long-axis distance is measured at the end of systole, from the centre of the tricuspid annulus to the centre of the superior RA wall (normal range for men 2.4 ± 0.3 cm/m^2 and 2.5 ± 0.3 cm/m^2 for women). The minor distance is measured at the mid-level of the RA, from the free wall to the interatrial septum (perpendicular to the RA long axis) (normal range for men and women 1.9 ± 0.3 cm/m^2).[18] The RA area can be derived by planimetry from the apical four-chamber view, and RA volumes are mostly reported from 2D echocardiography (normal range 21 ± 6 mL/ m^2 for women and 25 ± 6 mL/ m^2 for men),[18] but ideally RA volume is assessed from three-dimensional (3D) echocardiography with higher accuracy and reproducibility than 2D echocardiography. Cardiac magnetic resonance (CMR) is the current 'gold standard' for volume quantification. Computed tomography (CT) has also been used recently for this purpose. Intracardiac echocardiography also allows detailed exploration of the RA structures and can be very useful for the safe accomplishment of transseptal puncture.[19]

3.1.1.2 Functional parameters

With tissue Doppler imaging (TDI), it is possible to directly measure the velocity of the atrial myocardium, where the a' reflects the contraction of the atrium. More recently, 2D strain measurements permit assessment of RA strain (active deformation).[20,21] These approaches have been used extensively for the LA, but limited data are available for the RA.

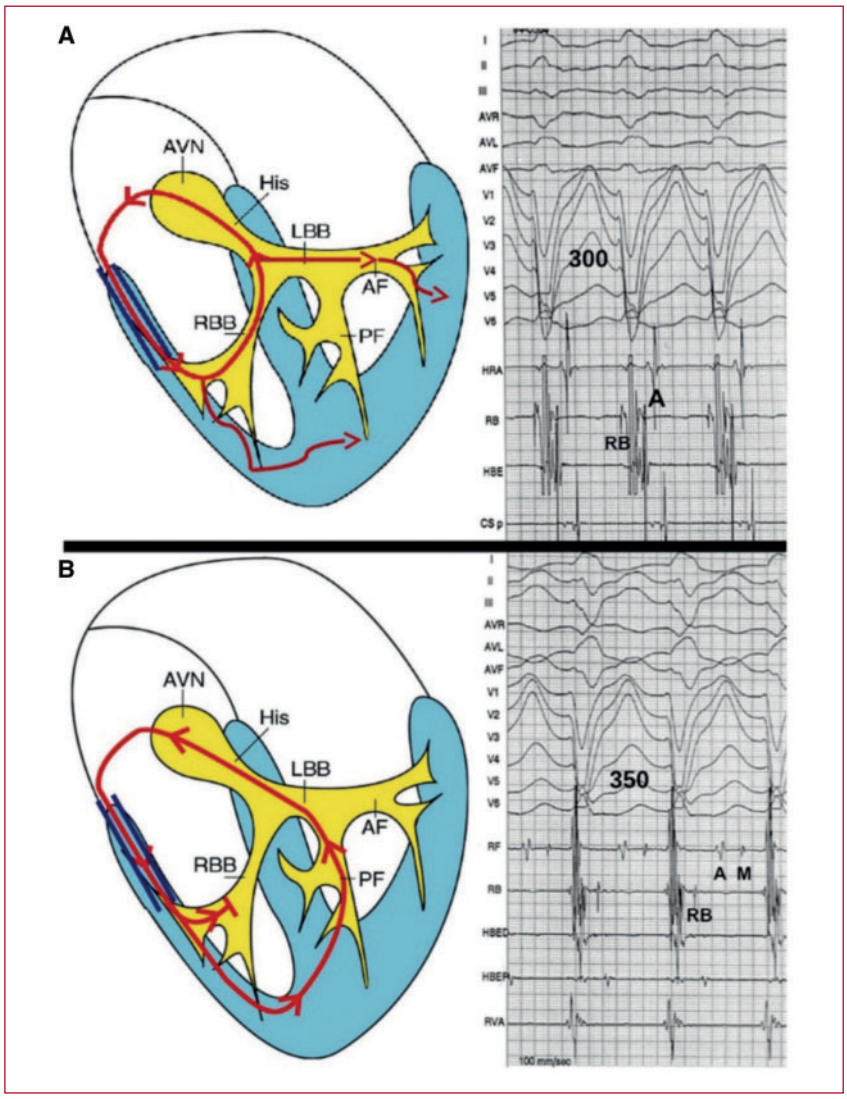

Supplementary Figure 5 Atypical pathway physiology. Change in QRS morphology from short to long ventriculoatrial atrioventricular re-entrant tachycardia. (*A*) During short ventriculoatrial atrioventricular re-entrant tachycardia (tachycardia cycle length 300 ms), there is also antegrade activation over the left anterior fascicle to produce a fused QRS complex with a normal axis. (*B*) With retrograde right bundle branch block, antegrade conduction over the left anterior fascicle is no longer possible and conduction to the left ventricle proceeds only via the right free wall. Therefore, the long ventriculoatrial atrioventricular re-entrant tachycardia (tachycardia cycle length 350 ms) has a leftward axis. During the change from short to long ventriculoatrial atrioventricular re-entrant tachycardia, the QRS width also increases from 120 to 150 ms. Reproduced with permission from Gandhavadi M *et al.*[13] A = atrial electrogram; AF = anterior fascicle; AVN = atrioventricular node; AVRT = atrioventricular re-entrant tachycardia; LBB = left bundle branch catheter; M = Mahaim potential; PF = posterior fascicle; RB = right bundle potential; RBB = right bundle branch catheter.

3D echocardiography has been used recently for the sophisticated assessment of atrial function. This technique allows precise quantification of volume shifts from the atrium to the LV and has been applied mainly for the LA.[18,21]

3.2 Left atrium

The LA is the most posteriorly situated heart chamber (*Supplementary Figure 7*). Internally, its smooth venous part receives the pulmonary veins (PVs) into the body of the chamber and its vestibule surrounds the opening to the mitral valve.[22] The great cardiac vein and its continuation into the coronary sinus lie outside, along the posteroinferior wall of the LA, and have variable extents of muscular continuity with the atrial wall.

The atrial wall has significant regional variations in muscular thickness. The superior wall (roof) is 3.5–6.5 mm thick while the anterosuperior wall augmented by Bachmann's bundle (interauricular muscle band) is even thicker. However, other regions can be as thin as 1–2 mm or nearly paper thin.[22]

The LA appendage is a flattened tubular structure with considerable variability in shape and size. It has a narrow opening (ostium) to the atrial body (*Supplementary Figure 7*). The tip of the appendage is

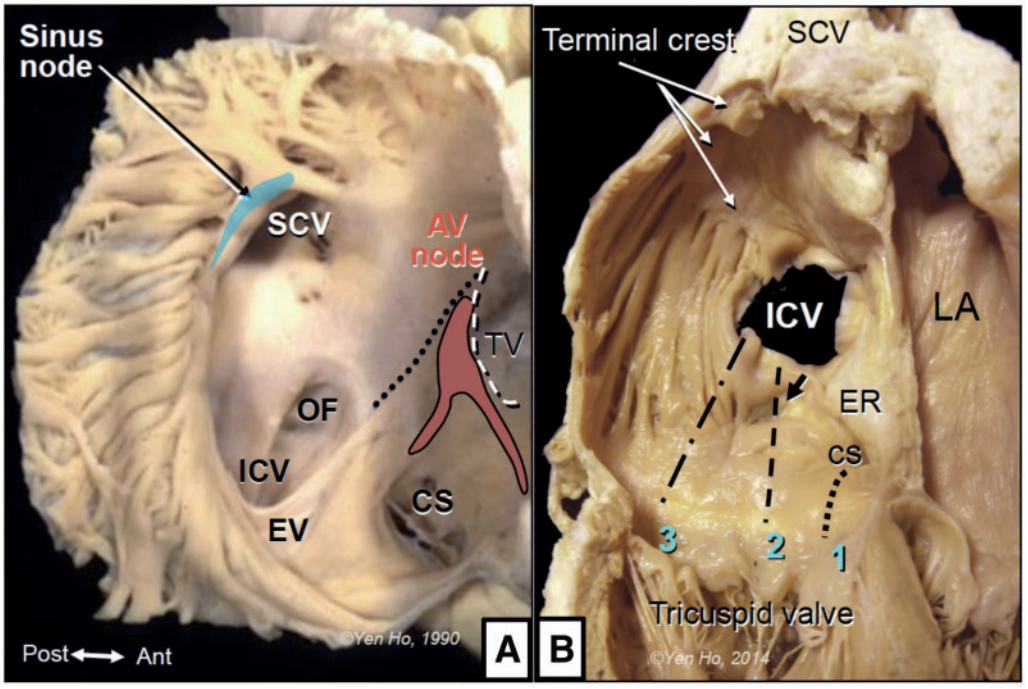

Supplementary Figure 6 Anatomy of the right atrium. (*A*) This display of the inside of the right atrium with the lateral wall of the appendage deflected posteriorly shows the atrial septum enface and the terminal crest with its array of pectinate muscles. The sinus and atrioventricular nodes are superimposed. The dotted line marks the position of the tendon of Todaro and the white broken line marks the annulus of the septal leaflet of the tricuspid valve, the borders of the triangle of Koch. (*B*) This four-chamber section shows three lines in the cavotricuspid isthmus corresponding to the paraseptal isthmus (1), inferior/central isthmus (2), and inferolateral isthmus (3). The short arrow indicates a pouch-like depression crossed by line 2. Courtesy of Dr Ho. AV = atrioventricular; CS = coronary sinus; ER = Eustachian ridge; EV = Eustachian valve; ICV = inferior caval vein; LA = left atrium; OF = oval fossa; SCV = superior caval vein; SN = sinus node; TC = terminal crest; TV = tricuspid valve.

commonly directed anteriorly, overlying the pulmonary trunk or the LV summit, where its floor sits on the early branches of the left coronary artery and the interventricular vein.[23]

Inside the atrium, a prominent left lateral ridge lies between the orifices of the left PVs and the ostium of the appendage (*Supplementary Figure* 7). Epicardially, the ridge is a fold containing the remnant of the oblique vein of Marshall with its accompanying autonomic nerves, and in some hearts also the artery supplying the sinus node.[22]

Although there are usually four pulmonary venous orifices, two on each side of the venous component, variations in the number of orifices, lengths of conjoined veins, and atypical locations are not uncommon.[24] The pulmonary venous trunk is defined as the distance from the orifice to the first-order branch. The superior PV orifices are larger and have a longer trunk (19–20 mm).[25]

Complex muscular architecture is found at the venoatrial junctions where the LA wall extends over the outer surface of the venous wall, creating muscular sleeves, longest along the upper veins.[26] The sleeves are thicker and circumferential at the venoatrial junctions, especially around the superior PVs, and thinner and more irregular towards the lung hilum. At the venoatrial junction, the veins connect through subepicardially and subendocardially located myocardial bridges crossing the interpulmonary isthmus.[22] The areas of the venoatrial junctions and adjoining PVs are also highly innervated by ganglionated nerves originating from the cardiac neural plexus.[27]

The phrenic nerves track along the lateral mediastinum, coursing along the outer surface of the fibrous pericardium. The right phrenic nerve has a close relationship with the superior caval vein and the anterior border of the orifice of the right superior PV. In the majority of individuals, the left phrenic nerve passes over the roof or the ostial wall of the LA appendage.[28] The oesophagus is located in close proximity to the posterior wall and the vagal plexus descends on its anterior surface (*Supplementary Figure* 7).[22] Furthermore, pericardial access is limited by pericardial sinuses and recesses around the veins and great arteries.

3.2.1 Non-invasive imaging of the left atrium

Non-invasive imaging can provide useful information on structural (anatomical) and/or functional abnormalities in the LA.[18,20,21,29]

3.2.1.1 Anatomical parameters

LA size and shape are typically assessed with standard 2D echocardiography, at the end of LV systole, before mitral valve opening. Dilatation is assessed by measuring the LA anteroposterior diameter (derived from the parasternal long-axis view); however, LA dilation in the anteroposterior direction is limited by the thorax, and dilation occurs mostly along the long axis of the LA. Therefore, assessment of LA volumes is preferred, which can be performed with 2D echocardiography; the reported normal values are 16 - 34 mL/m^2 for both

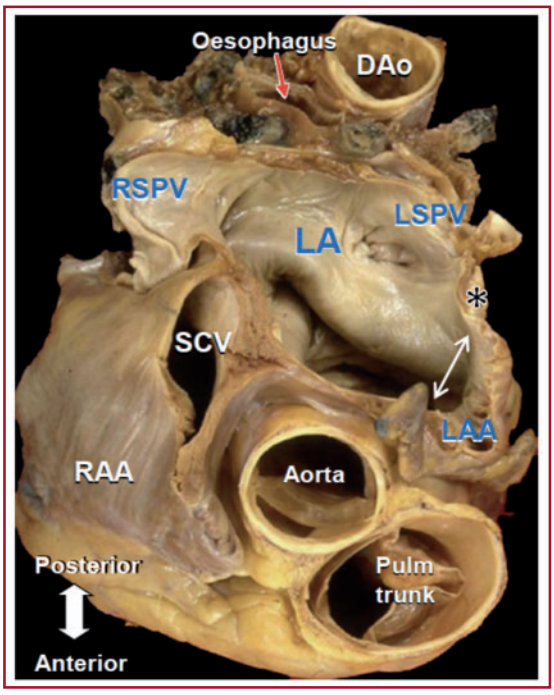

Supplementary Figure 7 Anatomy of the left atrium. The left atrium of this heart has been cut in a plane along the short axis of the thorax through the orifices of the right and left superior pulmonary veins. The double-headed arrow marks the ostium of the left atrial appendage, while the asterisk marks the ridge. The oesophagus and descending aorta pass behind the left atrium. Courtesy of Dr Ho. DAo = descending aorta; LA = left atrium; LAA = left atrial appendage; LSPV = left superior pulmonary vein; RAA = right atrial appendage; RSPV = right superior pulmonary vein; SCV = superior caval vein.

men and women. Higher-resolution 3D imaging techniques to assess LA volumes include 3D echocardiography, CMR, and CT. The reported normal volume values according to 3D echocardiography are 15–42 mL/m^2 in men and 15–39 mL/m^2 in women (slightly higher than 2D echocardiography).[18]

LA fibrosis has been assessed with echocardiography using integrated backscatter, where greater reflectivity indicates more fibrosis.[21,29] Reduced LA strain has also been related to LA fibrosis, as well as late gadolinium contrast-enhanced CMR; the contrast agent accumulates in the extracellular space (fibrosis) in the LA, appearing as white regions on the CMR images.[21,29] This might enable estimation of the extent of fibrosis in the LA,[30] which has been related to AF recurrence after ablation. However, this assessment depends on the method applied for the visualization of fibrosis and scarring using CMR.[31]

3.2.1.2 Functional parameters

LA function can be measured indirectly with pulsed-wave Doppler echocardiography (E and A waves reflecting blood flow velocity over the mitral valve in diastole).[21] The E wave represents passive flow from the PVs to the LV, whereas the A wave is the result of active atrial contraction (with reducing velocity indicating less contraction, which can relate to more LA fibrosis).[21,29] With increasing age, the A wave decreases.

From the colour-coded tissue Doppler images, the PA-TDI interval [P-wave on the (ECG) to peak a' on TDI] reflects the electromechanical delay (reflecting LA fibrosis) and predicts future AF. Also, the use of 2D echo strain imaging has been used to assess active deformation, which provides further insights into LA function.[20] Recently, 3D echocardiography has been used for sophisticated assessment of LA function: reservoir function is related to increased LA fibrosis, indicating less distensibility secondary to LA fibrosis.[20,21,29]

Delayed-enhancement CMR has also been introduced for the assessment of atrial fibrosis.[30]

3.3 Conduction tissues

The sinus node is located in the terminal crest at the anterolateral border of the entrance of the superior caval vein (*Supplementary Figure 6*). Tadpole-shaped, with a broad head portion and a tapering tail, it extends superiorly from the subepicardial location and penetrates inferiorly into the terminal crest with its tail toward the subendocardium.[32]

The triangle of Koch on the endocardial aspect of the RA is an established guide to the location of the atrioventricular (AV) conduction tissues.[14] Its posterior border is the tendon of Todaro within the Eustachian ridge, while its anterior border is the annulus of the septal leaflet of the tricuspid valve, and the orifice of the coronary sinus marks its base. The AVN and bundle lie at its apex, while the orifice of the coronary sinus marks its base (*Supplementary Figure 6*). The inferior extensions of the compact AVN are thought to account for the slow pathway in nodal re-entry tachycardia, although the arrangement of the cardiomyocytes in this area may also play a role.[33]

As there are no histologically specialized conduction tissues between the sinus and AVNs, the sinus impulse is transmitted preferentially toward the AVN via muscle bundles with a well-aligned arrangement of cardiomyocytes, and thence into the ventricles through the AV conduction system.[14]

3.4 Accessory pathways

Atrial and ventricular myocardial masses are separated at the AV junction by a tissue plane of fibro-fatty tissues at the annulus of the tricuspid and mitral valves, and at the septum. Breaches of this insulating tissue plane by myocardial bundles of varying sizes, morphologies, and number constitute AV APs that allow the atrial impulse to reach the ventricular mass, bypassing the AV conduction system.[34] A detailed discussion can be found in section 11.3 of the main text.

4 References

1. Wit AL, Wellens HJ, Josephson ME. *Electrophysiological Foundations of Cardiac Arrhythmias*. 1st ed. Minneapolis: Cardiotext Publishing; 2017.
2. Qu Z, Xie LH, Olcese R, Karagueuzian HS, Chen PS, Garfinkel A, Weiss JN. Early afterdepolarizations in cardiac myocytes: beyond reduced repolarization reserve. *Cardiovasc Res* 2013;**99**:6–15.
3. Zaza A, Rocchetti M. Calcium store stability as an antiarrhythmic endpoint. *Curr Pharm Des* 2015;**21**:1053–1061.
4. Vaquero M, Calvo D, Jalife J. Cardiac fibrillation: from ion channels to rotors in the human heart. *Heart Rhythm* 2008;**5**:872–879.
5. Roberts-Thomson KC, Kistler PM, Kalman JM. Focal atrial tachycardia I: clinical features, diagnosis, mechanisms, and anatomic location. *Pacing Clin Electrophysiol* 2006;**29**:643–652.
6. Goette A, Kalman JM, Aguinaga L, Akar J, Cabrera JA, Chen SA, Chugh SS, Corradi D, D'Avila A, Dobrev D, Fenelon G, Gonzalez M, Hatem SN, Helm R,

Hindricks G, Ho SY, Hoit B, Jalife J, Kim Y-H, Lip GYH, Ma C-S, Marcus GM, Murray K, Nogami A, Sanders P, Uribe W, Van Wagoner DR, Nattel S. EHRA/HRS/APHRS/SOLAECE expert consensus on atrial cardiomyopathies: definition, characterization, and clinical implication. *Heart Rhythm* 2017;**14**:e3–e40.
7. Zhang XD, Timofeyev V, Li N, Myers RE, Zhang DM, Singapuri A, Lau VC, Bond CT, Adelman J, Lieu DK, Chiamvimonvat N. Critical roles of a small conductance Ca(2)(+)-activated K(+) channel (SK3) in the repolarization process of atrial myocytes. *Cardiovasc Res* 2014;**101**:317–325.
8. Limberg SH, Netter MF, Rolfes C, Rinne S, Schlichthorl G, Zuzarte M, Vassiliou T, Moosdorf R, Wulf H, Daut J, Sachse FB, Decher N. TASK-1 channels may modulate action potential duration of human atrial cardiomyocytes. *Cell Physiol Biochem* 2011;**28**:613–624.
9. Burashnikov A, Di Diego JM, Zygmunt AC, Belardinelli L, Antzelevitch C. Atrium-selective sodium channel block as a strategy for suppression of atrial fibrillation: differences in sodium channel inactivation between atria and ventricles and the role of ranolazine. *Circulation* 2007;**116**:1449–1457.
10. Kirchhof PF, Fabritz CL, Franz MR. Postrepolarization refractoriness versus conduction slowing caused by class I antiarrhythmic drugs: antiarrhythmic and proarrhythmic effects. *Circulation* 1998;**97**:2567–2574.
11. Yin H, el-Sherif N, Caref EB, Ndrepepa G, Levin R, Isber N, Stergiopolus K, Assadi MA, Gough WB, Restivo M. Actions of lidocaine on reentrant ventricular rhythms in the subacute myocardial infarction period in dogs. *Am J Physiol* 1997;**272**:H299–H309.
12. Katritsis DG, Marine JE, Contreras FM, Fujii A, Latchamsetty R, Siontis KC, Katritsis GD, Zografos T, John RM, Epstein LM, Michaud GF, Anter E, Sepahpour A, Rowland E, Buxton AE, Calkins H, Morady F, Stevenson WG, Josephson ME. Catheter ablation of atypical atrioventricular nodal reentrant tachycardia. *Circulation* 2016;**134**:1655–1663.
13. Gandhavadi M, Sternick EB, Jackman WM, Wellens HJ, Josephson ME. Characterization of the distal insertion of atriofascicular accessory pathways and mechanisms of QRS patterns in atriofascicular antidromic tachycardia. *Heart Rhythm* 2013;**10**:1385–1392.
14. Ho SY, Anderson RH, Sánchez-Quintana D. Atrial structure and fibres: morphologic bases of atrial conduction. *Cardiovasc Res* 2002;**54**:325–336.
15. Ueda A, McCarthy KP, Sánchez-Quintana D, Yen Ho S. Right atrial appendage and vestibule: further anatomical insights with implications for invasive electrophysiology. *Europace* 2013;**15**:728–734.
16. Cabrera JA, Sanchez-Quintana D, Farre J, Rubio JM, Ho SY. The inferior right atrial isthmus: further architectural insights for current and coming ablation technologies. *J Cardiovasc Electrophysiol* 2005;**16**:402–408.
17. Tadic M. The right atrium, a forgotten cardiac chamber: an updated review of multimodality imaging. *J Clin Ultrasound* 2015;**43**:335–345.
18. Lang RM, Badano LP, Mor-Avi V, Afilalo J, Armstrong A, Ernande L, Flachskampf FA, Foster E, Goldstein SA, Kuznetsova T, Lancellotti P, Muraru D, Picard MH, Rietzschel ER, Rudski L, Spencer KT, Tsang W, Voigt JU. Recommendations for cardiac chamber quantification by echocardiography in adults: an update from the American Society of Echocardiography and the European Association of Cardiovascular Imaging. *J Am Soc Echocardiogr* 2015;**28**:1–39.e14.
19. Enriquez A, Saenz LC, Rosso R, Silvestry FE, Callans D, Marchlinski FE, Garcia F. Use of intracardiac echocardiography in interventional cardiology: working with the anatomy rather than fighting it. *Circulation* 2018;**137**:2278–2294.
20. Badano LP, Kolias TJ, Muraru D, Abraham TP, Aurigemma G, Edvardsen T, D'Hooge J, Donal E, Fraser AG, Marwick T, Mertens L, Popescu BA, Sengupta PP, Lancellotti P, Thomas JD, Voigt JU. Standardization of left atrial, right ventricular, and right atrial deformation imaging using two-dimensional speckle tracking echocardiography: a consensus document of the EACVI/ASE/Industry Task Force to standardize deformation imaging. *Eur Heart J Cardiovasc Imaging* 2018;**19**:591–600.
21. Delgado V, Di Biase L, Leung M, Romero J, Tops LF, Casadei B, Marrouche N, Bax JJ. Structure and function of the left atrium and left atrial appendage: AF and stroke implications. *J Am Coll Cardiol* 2017;**70**:3157–3172.
22. Ho SY, Cabrera JA, Sanchez-Quintana D. Left atrial anatomy revisited. *Circ Arrhythm Electrophysiol* 2012;**5**:220–228.
23. Su P, McCarthy KP, Ho SY. Occluding the left atrial appendage: anatomical considerations. *Heart* 2008;**94**:1166–1170.
24. Kato R, Lickfett L, Meininger G, Dickfeld T, Wu R, Juang G, Angkeow P, LaCorte J, Bluemke D, Berger R, Halperin HR, Calkins H. Pulmonary vein anatomy in patients undergoing catheter ablation of atrial fibrillation: lessons learned by use of magnetic resonance imaging. *Circulation* 2003;**107**:2004–2010.
25. Cronin P, Sneider MB, Kazerooni EA, Kelly AM, Scharf C, Oral H, Morady F. MDCT of the left atrium and pulmonary veins in planning radiofrequency ablation for atrial fibrillation: a how-to guide. *AJR Am J Roentgenol* 2004;**183**:767–778.
26. Ho SY, Cabrera JA, Tran VH, Farre J, Anderson RH, Sanchez-Quintana D. Architecture of the pulmonary veins: relevance to radiofrequency ablation. *Heart* 2001;**86**:265–270.
27. Chevalier P, Tabib A, Meyronnet D, Chalabreysse L, Restier L, Ludman V, Aliès A, Adeleine P, Thivolet F, Burri H, Loire R, François L, Fanton L. Quantitative study of nerves of the human left atrium. *Heart Rhythm* 2005;**2**:518–522.
28. Sanchez-Quintana D, Ho SY, Climent V, Murillo M, Cabrera JA. Anatomic evaluation of the left phrenic nerve relevant to epicardial and endocardial catheter ablation: implications for phrenic nerve injury. *Heart Rhythm* 2009;**6**:764–768.
29. Donal E, Lip GY, Galderisi M, Goette A, Shah D, Marwan M, Lederlin M, Mondillo S, Edvardsen T, Sitges M, Grapsa J, Garbi M, Senior R, Gimelli A, Potpara TS, Van Gelder IC, Gorenek B, Mabo P, Lancellotti P, Kuck KH, Popescu BA, Hindricks G, Habib G, Cardim NM, Cosyns B, Delgado V, Haugaa KH, Muraru D, Nieman K, Boriani G, Cohen A. EACVI/EHRA Expert Consensus Document on the role of multi-modality imaging for the evaluation of patients with atrial fibrillation. *Eur Heart J Cardiovasc Imaging* 2016;**17**:355–383.
30. Gal P, Marrouche NF. Magnetic resonance imaging of atrial fibrosis: redefining atrial fibrillation to a syndrome. *Eur Heart J* 2017;**38**:14–19.
31. Karim R, Housden RJ, Balasubramaniam M, Chen Z, Perry D, Uddin A, Al-Beyatti Y, Palkhi E, Acheampong P, Obom S, Hennemuth A, Lu Y, Bai W, Shi W, Gao Y, Peitgen HO, Radau P, Razavi R, Tannenbaum A, Rueckert D, Cates J, Schaeffter T, Peters D, MacLeod R, Rhode K. Evaluation of current algorithms for segmentation of scar tissue from late gadolinium enhancement cardiovascular magnetic resonance of the left atrium: an open-access grand challenge. *J Cardiovasc Magn Reson* 2013;**15**:105.
32. Ho SY, Sánchez-Quintana D. Anatomy and pathology of the sinus node. *J Interv Card Electrophysiol* 2016;**46**:3–8.
33. Katritsis DG, Becker A. The atrioventricular nodal reentrant tachycardia circuit: a proposal. *Heart Rhythm* 2007;**4**:1354–1360.
34. Ho SY. Accessory atrioventricular pathways: getting to the origins. *Circulation* 2008;**117**:1502–1504.